AIP | Applied Physics Letters

Impact of vacancy clusters on characteristic resistance change of nonstoichiometric strontium titanate nano-film

Yong Su Kim, Jiyeon Kim, Moon Jee Yoon, Chang Hee Sohn, Shin Buhm Lee, Daesu Lee, Byung Chul Jeon, Hyang Keun Yoo, Tae Won Noh, Aaron Bostwick, Eli Rotenberg, Jaejun Yu, Sang Don Bu, and Bongjin Simon Mun

Citation: Applied Physics Letters **104**, 013501 (2014); doi: 10.1063/1.4860961
View online: http://dx.doi.org/10.1063/1.4860961
View Table of Contents: http://scitation.aip.org/content/aip/journal/apl/104/1?ver=pdfcov
Published by the AIP Publishing

Impact of vacancy clusters on characteristic resistance change of nonstoichiometric strontium titanate nano-film

Yong Su Kim,[1,a)] Jiyeon Kim,[2] Moon Jee Yoon,[1] Chang Hee Sohn,[1] Shin Buhm Lee,[1] Daesu Lee,[1] Byung Chul Jeon,[1] Hyang Keun Yoo,[1] Tae Won Noh,[1] Aaron Bostwick,[3] Eli Rotenberg,[3] Jaejun Yu,[2] Sang Don Bu,[4] and Bongjin Simon Mun[5]

[1]*CFI-CES, IBS and Department of Physics & Astronomy, Seoul National University, Seoul 151-747, South Korea*

[2]*CSCMR, Department of Physics and Astronomy, Seoul National University, Seoul 151-747, South Korea*

[3]*Advanced Light Source, Lawrence Berkeley National Laboratory, Berkeley, California 94720, USA*

[4]*Department of Physics, Chonbuk National University, Jeonju 561-756, South Korea*

[5]*Department of Physics & Photon Science, School of Physics & Chemistry, Ertl Center for Electrochemistry and Catalyst, Gwangju Institute of Science and Technology, Gwangju 500-712, South Korea*

(Received 26 August 2013; accepted 15 December 2013; published online 2 January 2014)

In practical applications to bipolar resistance switching (BRS) memory devices with enhanced performance and high-scalability, oxide materials are commonly fabricated to highly nonstoichiometric and nanometer scale films. In this study, we fabricated ultrathin strontium titanate film, which shows two types of BRS behavior. By using micro-beam X-ray photoemission spectroscopy, the changes of core-level spectra depending on the resistance states are spatially resolved. Experimental and calculated results demonstrated that the fundamental switching mechanism in the two types of BRS is originated from the migration of anion and cation vacancies and the formation of insulating vacancy clusters near vicinity of the interface. © *2014 AIP Publishing LLC*. [http://dx.doi.org/10.1063/1.4860961]

One of the newly emerging properties exhibited by oxide materials is the resistance-switching (RS) phenomenon. By applying external voltages, oxide RS materials exhibit reversible resistance switching between a high resistance state (HRS) and a low resistance state (LRS).[1–3] These oxide materials, with electrically controllable bistable states, have drawn considerable attention as promising candidates for next-generation nonvolatile memory devices.

Between the two kinds of RS materials, unipolar RS (URS)[1,4] and bipolar RS (BRS),[1,5] most of the research has indicated that BRS materials are more promising for high-scalability applications. However, due to the phenomenological diversity of BRS, questions still remain regarding the feasibility of using this material, which should be clarified before practical application. For example, so far, two types of switching polarities have been observed in BRS materials.[6–8] Specifically, when a positive voltage is applied, some samples show current–voltage (I–V) curves with a clockwise rotation in the first quadrant (i.e., from LRS to HRS),[6,7,9] which is also referred to as the "counter-figure-8" rotation. On the other hand, other samples show I–V curves with a counterclockwise rotation (i.e., from HRS to LRS) in the first quadrant, which is also known as the "figure-8" rotation.[6,8,9] The differences in the switching behavior of oxide BRS materials have been attributed to defects. Even the purest crystals have defects, such as vacancies. Moreover, in practical applications to RS memory devices with enhanced performance and scalability, oxide materials are commonly fabricated to highly nonstoichiometric and nanometer-scale films. Therefore, an understanding of the roles of defects in oxide nano-thin film is important for the RS application.

Oxygen vacancies are considered to be the most critical defects in the RS phenomena occurring in oxide systems.[9–11] The oxygen vacancy is a positively charged defect. When a negative voltage is applied, oxygen vacancies migrate towards the metal–oxide film interface, depleting oxygen near the interface. Such changes in oxygen distribution could result in bistable states, which are used in the RS. However, the oxygen vacancy model, which assumes that only the oxygen vacancies can move under an applied electric field, might not be sufficient to describe BRS in many oxide materials. Oxide ultrathin films, particularly nonstoichiometric samples, usually contain both cation and anion vacancies. With a high density of vacancies, it is energetically favorable to form various types of defect clusters,[12,13] each of which has different physical properties. Therefore, to understand RS, especially in nonstoichiometric oxides ultrathin film, the effects of defect clusters, as well as point vacancies, should be accounted for. However, to date, there have been few investigations on the roles of defect clusters in RS phenomena.

Here, we investigated the RS phenomena of nonstoichiometric strontium titanate films. Applied voltage pulses were used to generate four resistance states, which were then probed by high-resolution X-ray photoelectron spectroscopy (HR-XPS). By combining the resistance states and HR-XPS data, we found that the simple motions of the O vacancy (V_O) and Sr vacancy (V_{Sr}) were not enough to explain the BRS of our ultrathin nonstoichiometric strontium titanate films. We then performed density functional theory (DFT) calculations, and found that the Sr–O–O vacancy cluster ($V_{Sr–O–O}$) can be easily formed by combining of the Sr–O vacancy ($V_{Sr–O}$) and V_O. Based on our experimental and theoretical works, we propose that the defects (vacancies and

[a)]ysukim@phya.snu.ac.kr

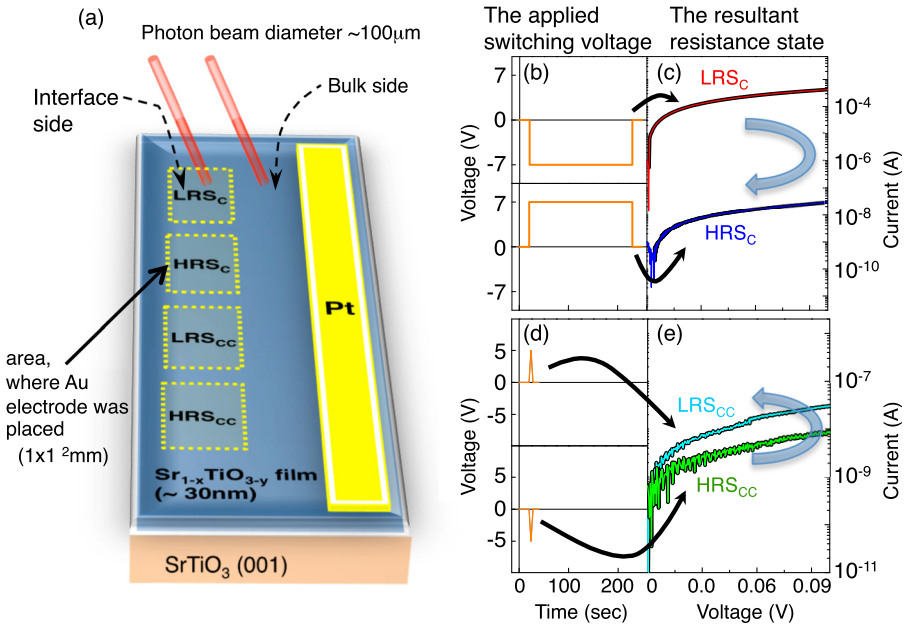

FIG. 1. (a) Schematic diagram of non-stoichiometric STO film on $SrTiO_3(001)$. (b) and (d) The applied voltage conditions for the four resistance states. (c) and (e) The resulting current levels of the four resistance states at 0.1 V reading voltage. The subscripts "C" and "CC" represent "clockwise-rotation" and "counterclockwise-rotation" of the *I–V* curve in the first quadrant, respectively.

vacancy clusters) play important roles in RS, especially for nonstoichiometric samples.

Figure 1(a) shows a schematic diagram of the geometry of the nonstoichiometric $Sr_{1-x}TiO_{3-y}$ film deposited on the $SrTiO_3(001)$ substrate and how we performed the HR-XPS measurements. We deposited 100-nm-thick nonstoichiometric strontium titanate film on $SrTiO_3(001)$ substrate by pulsed laser deposition with *in-situ* reflection high-energy electron diffraction. During deposition, the substrate temperature was 600 °C, and the oxygen partial pressure was 1×10^{-7} Torr. To prepare four resistance states before the HR-XPS measurement, we fabricated the planar metal-insulator-metal structure. On top of the nonstoichiometric strontium titanate film, we deposited a large Pt rectangular bar (5 mm × 3 mm) and a series of small Au squares (1 mm × 1 mm). On each of the Au electrodes, we applied an external voltage (i.e., positive and negative voltage) to prepare the four resistance states: LRS_i and HRS_i. Then, we removed the small Au electrodes and measured HR-XPS measurements.

We generated four resistance states by applying voltage pulses with different magnitude and duration. We applied a short-low voltage using an Agilent 4155C semiconductor-parameter analyser controlled by LabVIEW. For applying a long-high voltage, we used a YOKOGAWA FG300 synthesised function generator and monitored the output current simultaneously throughout the cell using a YOKOGAWA DL7100 digital oscilloscope. Figures 1(b) and 1(d) show the detailed shapes of the applied voltage pulses. We confirmed the resulting resistance states by measuring the current up to 0.1 V, as shown in Figs. 1(c) and 1(e). When a long–high–-negative voltage pulse (i.e., −7 V for 210 s) was applied, it entered to LRS_C. By then applying a positive voltage pulse (i.e., +7 V for 210 s), the resistance returned its original state, i.e., from LRS_C to HRS_C, as displayed in Figs. 1(b) and 1(c). Here, the subscript "C" represents "clockwise rotation," because the resulting *I–V* curve exhibited a clockwise rotation in the first quadrant. In contrast, we obtained the other two resistance states by applying short–low voltage pulses (±5 V triangular pulses for 15 s), as displayed in Figs. 1(d) and 1(e). We denote these resistance states as HRS_{CC} and LRS_{CC}. Here, the subscript "CC" represents "counterclockwise rotation," because the resulting *I–V* curve exhibited a counterclockwise rotation in the first quadrant. These results clearly demonstrated that the switching polarity of BRS in our nonstoichiometric strontium titanate film depended not only on the applied voltage polarity, but also on the applied voltage duration and intensity. Note that the resistance changes in Figs. 1(d) and 1(e) are counterintuitive in the oxygen vacancy model (see Fig. S1).[14]

To investigate the correlation between resistance states and chemical changes in the nonstoichiometric strontium titanate film, which is possibly due to the cation and anion migration driven by external voltages, we measured the core-level spectra of Sr, Ti, and O for the four resistance states using HR-XPS. The HR-XPS measurements were performed at beamline 7.0.1 of the Advanced Light Source at the Lawrence Berkeley National Laboratory. The hemispherical electron analyzer, Sicenta R4000, was used. The total energy resolution of the XPS spectra is set to below 0.1 eV.

It was very important to determine whether RS mainly originated from changes near the interface or inside the film bulk region, because this would provide a crucial guideline for designing and developing RS devices. Therefore, in our comparative study, we measured the core-level spectra on the interface side (where the Au top-electrode was originally placed) and also on the bulk side (in the region between the Au top- and Pt bottom-electrode).

Figure 2 shows that the O 1*s* and the Sr 3*d* core-level spectra of the four resistance states, obtained after background subtraction and normalization, on the bulk side. The O and Sr spectra consist of three and two components, respectively. For O 1*s*, the peaks ~529.5 and ~531.95 eV correspond to bulk oxygen inside the film and characteristic trace of carbonate adsorbate on the film surface.[15] The middle peak ~530.95 eV corresponds to the surface oxygen in the termination layer. The Sr $3d_{2/5}$ ($3d_{2/3}$) peak ~132.7 eV (~134.45 eV) can be attributed to the Sr bulk peak. The

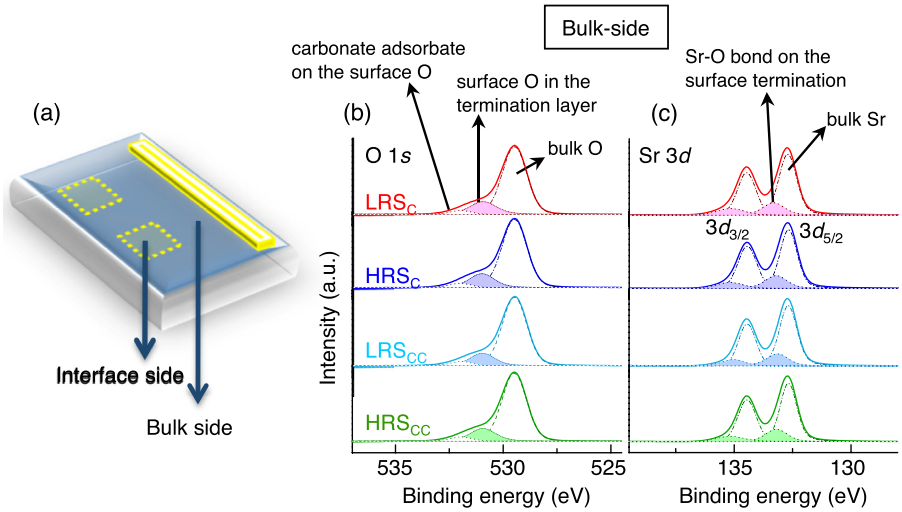

FIG. 2. (a) Schematic diagram of nonstoichiometric strontium titanate film on $SrTiO_3$(001) substrate. (b) O 1*s* and (c) Sr 3*d* core-level spectra measured on the bulk side with photon energies of 650 and 300 eV, respectively. The O 1*s* spectra consist of three components. The first (dotted), second (short-dashed), and third (dashed-dotted) (in order from the highest to the lowest binding energy components) correspond to the characteristic trace of carbonate adsorbate on the film surface, the surface oxygen in the termination layer, and bulk oxygen inside the film, respectively. The Sr 3*d* spectra display two peaks. The peak at the high and the low binding energy sides correspond to the Sr bulk and Sr–O bond at the surface termination layer, respectively.

peaks ~133.35 and ~135.1 eV represent the Sr–O bond at the surface termination layer.[15,16]

Interestingly, as displayed in Fig. 2, the core-level spectra of O 1*s* and Sr 3*d* on the bulk side do not show any significant changes. On the other hand, interface side results display considerable differences among the four resistance states (these results will be presented below). These observations indicate that only the changes near the metal–oxide interface should play important roles for RS in nonstoichiometric strontium titanate ultrathin films.

Figures 3(e)–3(h) show that the O 1*s* core-level spectra of the four resistance states at the interface side, obtained after background subtraction and normalization. As stated above, each O 1*s* core-level spectrum has three components, which are displayed with dotted lines after the curve fittings. Among them, the middle peak, which is represented by the shaded area, corresponds to the surface oxygen in the termination layer. This peak becomes suppressed for LRS_C and HRS_{CC} states, both of which were obtained by applying negative voltages. This suggests that oxygen can be moved out of the interfacial region under the application of a negative voltage.

Figures 3(i)–3(l) show that the Sr 3*d* core-level spectra of the four resistance states at the interface side. The peaks, as illustrated by the shaded region, represent the Sr–O bond at the surface termination layer.[15,16] Note that this peak increases when the amount of oxygen and/or strontium at the surface increases and eventually forms a Sr–O termination layer. In the XPS results, surface component peak of Sr 3*d* was enhanced only at the short–low–positive voltage. When a short–low–positive voltage is applied, only V_O migrates away from the interface (i.e., O-atom moves toward the surface). But because there is no V_{Sr} movement, the Sr density is maintained. This indicates that interface region should have more oxygen and abundant O can form SrO on the surface termination. Because the diffusible oxygen on the surface migrates into the bulk under an applied negative voltage, the Sr–O peak in Figs. 3(i) and 3(l) shows no response. In contrast, it is interesting that the Sr–O peak of HRS_C [Fig. 3(j)] shows no enhanced response. This result suggests that Sr at the surface layer can be moved into the bulk region when the long–high–positive voltage was applied.[17–19]

Now, let us try to understand the resistance changes of LRS_C, HRS_C, LRS_{CC}, and HRS_{CC} from our HR-XPS measurements. From Figs. 1(c) and 1(e), we obtained the resistance values of the four states. Before the HR-XPS measurements, we confirmed the resistance levels by the

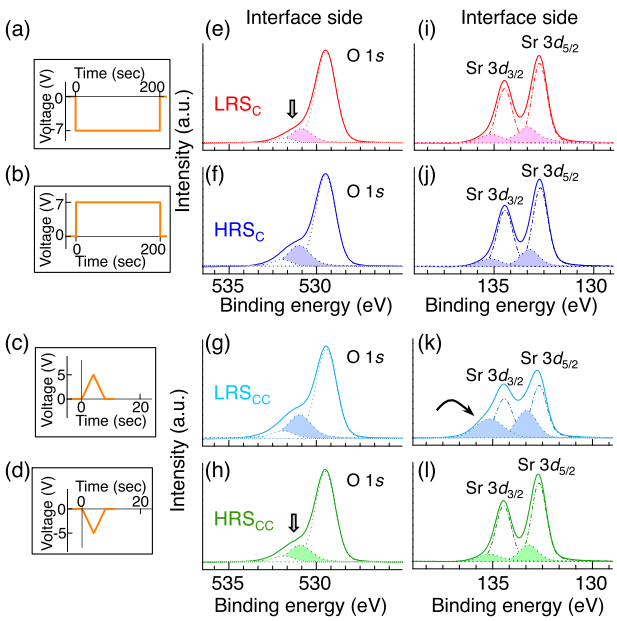

FIG. 3. HR-XPS core-level spectra of (a)–(d) the applied voltage pulses for each resistance state. (e)–(h) O 1*s* and (i)–(l) Sr 3*d*, taken with photon energies of 650 and 300 eV, respectively. The curve-fits with shaded areas in the O 1*s* and Sr 3*d* spectra represent the surface oxygen and Sr–O bond on the surface termination layer, respectively. For the long–high voltage application, migration of V_O and V_{Sr} near the interface induces LRS_C and HRS_C. The short–low voltage application only activates the V_O migration. In this case, the formation of V_{Sr-O-O} clusters generates HRS_{CC} and LRS_{CC}.

current reading at 0.1 V: 2.4×10^2 Ω for LRS_C, 3.5×10^6 Ω for HRS_C, 4.3×10^6 Ω for LRS_{CC}, and 3.5×10^7 Ω for HRS_{CC}. Based on the V_O and V_{Sr} migration model, the resistance states resulting from the applied high voltage can be understood. When a long–high–negative voltage is applied, positively charged V_O moves towards the interface, and negatively charged V_{Sr} moves away from the interface. Therefore, the region near the interface becomes rich in V_O and the lowest resistance state, LRS_C. When applying a long–high–positive voltage, V_{Sr} and V_O move in the opposite direction to that described above. In this case, the region near the interface becomes rich in V_{Sr}, which is not the major carrier source. It should be noted in this case is that because the formation energy of V_{Sr} is relatively higher than that of V_O,[12] the V_{Sr} density is less than the V_O density. Additionally, the migration of V_{Sr} is more limited,[19] compared with that of V_O. This implies the higher resistance state, HRS_C. However, this simple argument based on V_O and V_{Sr} does not agree with the observed results for the resistance states resulting from a low applied voltage, particularly, when HRS_{CC} has the highest resistance.

To investigate the formation of vacancy clusters, we performed DFT calculations using the Vienna *ab initio* Simulation Package (VASP) code.[20] The calculations were performed using the projector augmented wave (PAW) method within the local density approximation (LDA). On-site Coulomb interaction ($U = 5$ eV) and exchange parameter ($J = 0.36$ eV) were used with the LDA + U method to account for localized Ti-3d orbitals.[21,22] The atomic coordinates were optimized until the Hellmann–Feynman force was below 0.01 eV/(Å)$^{-1}$. We constructed a $4 \times 4 \times 4$ supercell based on the cubic phase of $SrTiO_3$.

To understand the creation of vacancies and vacancy clusters in the reduced condition of our nonstoichiometric strontium titanate films, fabricated at low oxygen pressure, we calculated the defect formation energies of various vacancy configurations.

The defect formation energy $E^f(X_q)$ for the defect X in a charge state q is calculated by[23]

$$E^f(X_q) = E_T(X_q) - E_T(0) - \Sigma_i n_i \mu_i + q(E_V + E_F). \quad (1)$$

$E_T(X_q)$ and $E_T(0)$ are the total energy of a supercell with defect and the total energy of perfect supercell, respectively. The formation energy depends on the chemical potential μ_i of atom type i, that is added to ($n_i > 0$) or removed from ($n_i < 0$) the perfect supercell. Here, n_i corresponds to the number of the defect atoms in the supercell. In addition, formation energy of charged defect depends on the Fermi level. Here, E_F corresponds to the Fermi energy measured from the valance band maximum as a reference point (E_V). The formation energies of single vacancies were found to be fully ionized states (V_{Sr}^{2+}, V_{Ti}^{4+}, and V_O^{2-}). For vacancy clusters, the transition levels were shown in the gap. For example, $V_{Sr–O–O}$ produces a transition level between the 2+ and 0 states. From extensive calculations, we determined the stability region of the chemical potential for the ternary Sr–Ti–O system. By choosing appropriate Sr, Ti, and O chemical potentials, we simulated the experimental "O-reduced condition" of strontium titanate films with high densities of V_{Sr}, V_O, and other vacancy clusters like $V_{Sr–O}$, $V_{O–O}$, and $V_{Sr–O–O}$.

In Fig. 4(a), we plotted the formation energy for vacancies (V_{Sr}, V_{Ti}, and V_O) and vacancy clusters ($V_{Sr–O}$, $V_{O–O}$, and $V_{Sr–O–O}$) as a function of the Fermi-level (E_F) in O-reduced condition. In this range of chemical potentials, while V_O and $V_{O–O}$ vacancies dominant for all values of E_F, the formation energies of V_{Sr}, V_O, $V_{O–O}$, $V_{Sr–O}$, and $V_{Sr–O–O}$ compete with each other when E_F reaches the bottom of the conduction band, i.e., in the electron doping limit.

To better understand the RS mechanism for the four resistance states, as presented in Figs. 3(a)–3(d), we calculated the binding energy of the vacancy clusters to estimate the possible formation process. Interestingly, the binding energies for the $V_{Sr} + V_O + V_O$ and $V_{Sr} + V_O$ vacancy clusters, 7.58 and 6.97 eV, respectively, are too high to expect the formation, while that for $V_{Sr–O} + V_O$ is sufficiently low for formation (0.61 eV). Therefore, we can expect that the formation of $V_{Sr–O–O}$ vacancy clusters from $V_{Sr–O} + V_O$ can easily occur.

There should be some amount of $V_{Sr–O}$ clusters inside our nonstoichiometric strontium titanate films. Namely, in all of the four resistance states, there are charge-neutral $V_{Sr–O}$ clusters. For oxygen-rich states, i.e., HRS_C and LRS_{CC}, $V_{Sr–O}$ vacancy clusters play a minor role in the resistance states. However, in HRS_{CC}, created by the

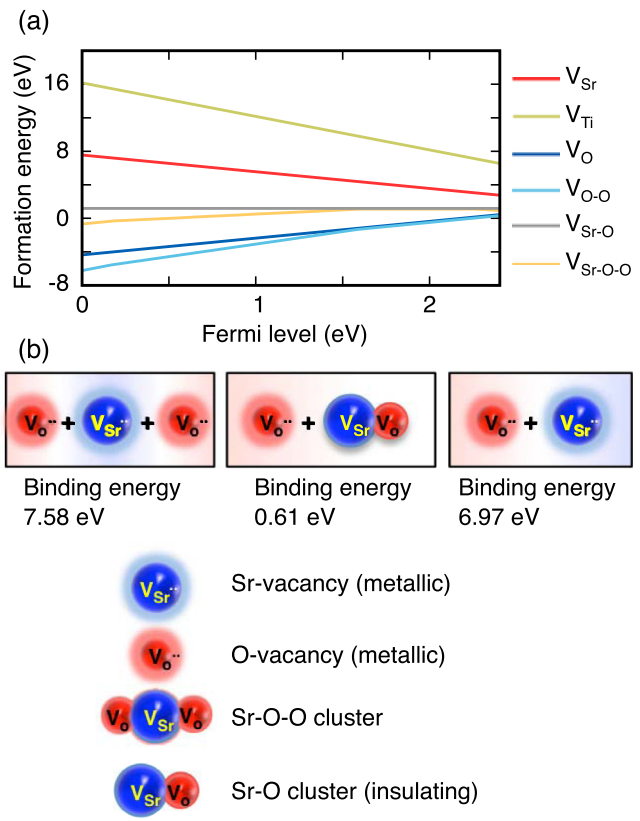

FIG. 4. (a) Formation energy as a function of the Fermi-level (E_F) for vacancies (V_{Sr}, V_{Ti}, and V_O) and vacancy clusters ($V_{Sr–O}$, $V_{O–O}$, and $V_{Sr–O–O}$) in the O-reduced condition. Here, atomic chemical potential is determined from Ti rich limit ($\mu_{Ti} = \mu_{Ti}$ (bulk), $2\mu_{Ti} + 3\mu_O = \mu_{Ti_2O_3}$ (bulk)). $E_F = 0$ corresponds to the top of the valence band varied up to 2.4 eV, which is the band gap energy of $SrTiO_3$. (b) Binding energy of the vacancy clusters obtained from the formation energy difference between the vacancy cluster and the dissociated vacancies.

application of a short-low-negative voltage pulse, most of the V_{Sr-O} vacancy clusters in the interfacial region could be combined with migrating V_O during the voltage pulse. Thus, this state would have the highest resistance. When a high voltage is applied, the considerable V_O can be easily migrated and the V_{Sr-O} clusters can be combined with migrating V_O to form the insulating product, V_{Sr-O-O}. However, because the V_O concentration is much higher than the V_{Sr-O} concentration, we expect there to be a surplus of oxygen vacancies; this is the reason why LRS_C should have the lowest resistance value. Namely, the formation of V_{Sr-O-O} vacancy clusters at low voltage should play an important role in determining the resistance property.

In summary, we investigated the RS phenomena of nonstoichiometric strontium titanate films. We found that V_O can move easily under applied external voltages. However a high and long external voltage pulse is required to move V_{Sr}. Simple arguments based on the motions of V_O and V_{Sr} cannot explain our resistance states and HR-XPS data. By combining these results with DFT calculations, we showed that V_{Sr-O} and V_{Sr-O-O} vacancy clusters play important roles in RS in our nonstoichiometric strontium titanate films. This work demonstrates the importance of defect clusters in the RS phenomena, especially in nonstoichiometric samples. In addition, this work suggested that the initial states (i.e., defect configurations and concentration) could be a very important factor for the switching rotations, especially nonstoichiometric oxide films.

This research was supported by the Institute of Basic Science (IBS) (EM 1203). B.S.M. would like to thank the support by Basic Science Research Program through the National Research Foundation of Korea (NRF) by the Ministry of Education, Science and Technology (MEST) (2012R1A1A2001745) and Accelerated Research Program (R17-2008-33-0100-0). The Advanced Light Source was supported by the Director, Office of Science, Office of Basic Energy Sciences, of the U.S. Department of Energy under Contract No. DE-AC02-05CH11231. This work was supported by PAL through the abroad beamtime program of Synchrotron Radiation Facility Project under MEST.

[1]R. Waser and M. Aono, Nature Mater. **6**, 833 (2007).
[2]J. Borghetti, G. S. Snider, P. J. Kuekes, J. J. Yang, D. R. Stewart, and R. S. Williams, Nature **464**, 873 (2010).
[3]M.-J. Lee, C. B. Lee, D. Lee, S. R. Lee, M. Chang, J. H. Hur, Y.-B. Kim, C.-J. Kim, D. H. Seo, S. Seo, U. I. Chung, I.-K. Yoo, and K. Kim, Nature Mater. **10**, 625 (2011).
[4]S. C. Chae, J. J. S. Lee, S. Kim, S. B. Lee, Sh. H. Chang, C. Liu, B. Kahng, H. Shin, D.-W. Kim, C. U. Jung, S. Seo, M.-J. Lee, and T. W. Noh, Adv. Mater. **20**, 1154 (2008).
[5]A. Sawa, Mater. Today **11**, 28 (2008).
[6]K. Shibuya, R. Dittmann, S. Mi, and R. Waser, Adv. Mater. **22**, 411 (2010).
[7]K. Szot, W. Speier, G. Bihlmayer, and R. Waser, Nature Mater. **5**, 312 (2006).
[8]A. Sawa, T. Fujii, M. Kawasaki, and Y. Tokura, Appl. Phys. Lett. **85**, 4073 (2004).
[9]F. Miao, J. J. Yang, J. Borghetti, G. Medeiros-Ribeiro, and R. S. Williams, Nanotechnology **22**, 254007 (2011).
[10]M. Janousch, G. I. Meijer, U. Staub, B. Delley, S. F. Karg, and B. P. Andreasson, Adv. Mater. **19**, 2232 (2007).
[11]R. Waser, R. Dittmann, G. Staikov, and K. Szot, Adv. Mater. **21**, 2632 (2009).
[12]Y. S. Kim, J. Kim, S. J. Moon, W. S. Choi, Y. J. Chang, J. G. Yoon, J. Yu, J. S. Chung, and T. W. Noh, Appl. Phys. Lett. **94**, 202906 (2009).
[13]Y. S. Kim, J. S. Choi, J. Kim, S. J. Moon, B. H. Park, J. Yu, J. H. Kwon, M. Kim, J. S. Chung, T. W. Noh, and J. G. Yoon, Appl. Phys. Lett. **97**, 242907 (2010).
[14]See supplementary material at http://dx.doi.org/10.1063/1.4860961 for point vacancy migration model.
[15]G. M. Vanacore, L. F. Zagonel, and N. Barrett, Surf. Sci. **604**, 1674 (2010).
[16]J. Szade, K. Szot, M. Kulpa, J. Kubacki, Ch. Lenser, R. Dittmann, and R. Waser, Phase Transitions **84**, 489 (2011).
[17]R. Meyer, R. Waser, J. Helmbold, and G. Borchardt, J. Electrocerm. **9**, 101 (2002).
[18]A. Walsh, C. R. A. Catlow, A. G. H. Smith, A. A. Sokol, and S. M. Woodley, Phys. Rev. B **83**, 220301 (2011).
[19]T. Mizoguchi, N. Takahashi, and H.-S. Lee, Appl. Phys. Lett. **98**, 091909 (2011).
[20]G. Kresse and D. Joubert, Phys. Rev. B **59**, 1758 (1999).
[21]S. L. Dudarev, G. A. Botton, S. Y. Savrasov, C. J. Humphreys, and A. P. Sutton, Phys. Rev. B **57**, 1505 (1998).
[22]D. D. Cuong, B. Lee, K. M. Choi, H.-S. Ahn, S. Han, and J. Lee, Phys. Rev. Lett. **98**, 115503 (2007).
[23]A. Janotti and C. G. V. Walle, Phys. Rev. B **76**, 165202 (2007).